ISSN 0005-1179 (print), ISSN 1608-3032 (online), Automation and Remote Control, 2023, Vol. 84, No. 10, pp. 1196–1210.

TOPICAL ISSUE

Increasing the Angular Resolution and Range of Measuring Systems Using Ultra-Wideband Signals

B. A. Lagovsky[*,a] **and E. Ya. Rubinovich**[**,b]

[*] *Russian Technological University (MIREA), Moscow, Russia*
[**] *Trapeznikov Institute of Control Sciences, Russian Academy of Sciences, Moscow, Russia*
e-mail: [a] *robertlag@yandex.ru,* [b] *rubinvch@gmail.com*

Received September 29, 2022
Revised July 23, 2023
Accepted August 2, 2023

Abstract—The problem of obtaining three-dimensional radio images of objects with increased resolution based on the use of ultra-wide-band pulse signals and new methods of their digital processing is considered. The inverse problem of reconstructing the image of a signal source with a resolution exceeding the Rayleigh criterion has been solved numerically. Mathematically, the problem is reduced to solving the Fredholm integral equation of the first kind by numerical methods based on the representation of the solution in the form of decomposition into systems of orthogonal functions. The method of selecting the systems of functions used, which increases the stability of solutions, is substantiated. Variational problems of optimizing the shape and duration of ultra-wide-band pulses have been solved, ensuring the maximum possible signal-to-noise ratio during location studies of objects with fully or partially known signal reflection characteristics. The proposed procedures make it possible to increase the range of measuring systems, and also make it possible to increase the stability of solutions to inverse problems. It is shown that the use of the developed methods for achieving super-resolution to process ultra-wideband signals dramatically improves the quality of 3D images of objects in the radio range.

Keywords: Rayleigh criterion, angular superresolution, stability of solutions to inverse problems

DOI: 10.25728/arcRAS.2023.90.53.001

1. INTRODUCTION

Increasing the effective angular resolution of radio and sonar, radio navigation, and remote sensing systems and bringing it to super-resolution makes it possible to detail images of the objects under study, solve problems of their recognition and identification, and separately observe individual targets as part of group targets. Solving these tasks makes it possible to improve the quality of existing and promising control systems for land, surface, underwater and aerospace objects. Currently, many methods of digital signal processing and analysis are known to increase the effective resolution. These are, in particular, methods of reverse convolution of signals, phase weighing coefficients, angular weighing, etc. Currently popular methods are: MUSIC (MUltiple SIgnal Classification) [1], ESPRIT (Estimation of Signal Parameters via Rotational Invariant Techniques) [2], deconvolution method [3, 4], maximum entropy method [5], maximum likelihood method [6], methods using neural networks [7], as well as nonlinear methods [8].

The listed methods are not effective in all cases. Most of them, including MUSIC and ESPRIT, turn out to be ineffective when active measuring systems use complex signals, in particular, UWB (Ultra Wide Band) signals with a duration of nanoseconds. The use of such ultra-wideband signals

potentially allows for very high resolution over a range of about 1 m. As a result, the combination of the use of UWB signals and the achievement of angular super-resolution due to digital signal processing will allow obtaining high-quality three-dimensional radio images of objects. Such systems are all-weather and can operate at any time of the day.

2. SETTING THE TASK OF ACHIEVING SUPER-RESOLUTION

The signal $U(\varphi,\theta)$ received by the goniometer system when scanning a two-dimensional sector of the survey can be expressed as a linear integral transformation [9]

$$U(\varphi,\theta)=\int\limits_{\Omega} f(\varphi-\phi,\theta-\vartheta)I(\phi,\vartheta)\,d\phi\,d\vartheta, \tag{1}$$

where $\Omega=\Omega(\varphi,\theta)$—the angular area of the signal source location; $I(\varphi,\theta)$—the angular amplitude distribution of the signal reflected (or emitted) by the object of observation, equal to zero outside Ω; $f(\varphi,\theta)$—directional pattern (DP) of the measuring system. For convenience, the Cartesian coordinate system is used here and further, where the angles are calculated from the normal to the antenna plane.

It is known that the angular resolution achieved during direct measurements in accordance with (1), i.e. the ability to distinguish two closely spaced objects, is measured by the minimum angles $\delta\varphi$ and $\delta\theta$, at which the two point signal sources still differ separately. These angles are determined based on the Rayleigh criterion

$$\delta\varphi\cong\lambda/D_x,\quad \delta\theta\cong\lambda/D_y, \tag{2}$$

where D_x and D_y are the linear dimensions of the antenna at the corresponding angles φ and θ directions, λ is a wavelength. The angles $\delta\varphi$ and $\delta\theta$ they turn out to be equal to the width of the DP, determined by reducing the radiated power by half and are denoted as $\varphi_{0.5}$ and $\theta_{0.5}$.

The task is to obtain an image of the signal source $I(\varphi,\theta)$ with an angular resolution exceeding the Rayleigh criterion to the greatest extent possible, based on the intelligent analysis of the received signal $U(\varphi,\theta)$ and the known DP $f(\varphi,\theta)$ of the system. Mathematically, the problem is reduced to an approximate solution of the Fredholm integral equation (IE) of the first kind of convolution type (1) with respect to an unknown function $I(\varphi,\theta)$ with the maximum achievable accuracy.

In general, attempts to increase the resolution exceeding (2) by solving the IE lead to unstable solutions, since the task belongs to the class of inverses and does not satisfy the second and third requirements of Hadamard correctness (2nd is an unambiguity of solutions and 3rd is their stability).

The methods of digital signal processing developed by the authors, called algebraic [9–15], seem promising, allowing to obtain a stable approximate solution of the IE (1).

3. ALGEBRAIC METHODS OF SOLUTION

Algebraic methods consist in parameterizing the problem by presenting approximate solutions in the form of expansions over selected sequences of functions. The choice of systems of functions is based on a priori information about the solution.

Let's consider practically important tasks when scanning is performed using one of the angular coordinates.

The desired distribution of $I(\varphi)$ can always be represented as a decomposition over some complete system of orthogonal functions in the domain of Ω $g_m(\varphi)$ with unknown coefficients b_m

$$I(\varphi)=\sum_{m=1}^{\infty} b_m g_m(\varphi)\cong\sum_{m=1}^{M} b_m g_m(\varphi). \tag{3}$$

Then the received signal is $U(\varphi)$ is expressed as a superposition of functions $G_m(\varphi)$, which are images of $g_m(\varphi)$ when converting

$$G_m(\varphi) = \int\limits_{\Omega} f(\varphi - \phi) g_m(\phi)\, d\phi, \tag{4}$$

$$U(\varphi) = \sum_{m=1}^{\infty} b_m G_m(\varphi) \cong \sum_{m=1}^{M} b_m g_m(\varphi), \tag{5}$$

where M is the selected number of expansion terms.

Thus, the inverse problem turns out to be parameterized, and its solution is reduced to finding the coefficients b_m [10–12], which are usually found when minimizing the standard deviation of the function $U(\varphi)$ from (5) from the signal under study (1) in the corner sector $\Phi > \Omega$, where Φ is the sector in which the useful signal exceeds noise and can be measured with sufficiently high accuracy. In practice, the boundaries of the Φ sector are often determined by reducing the amplitude of the useful signal by half in relation to its maximum value.

Function system $G_m(\varphi)$ of (4), generally speaking, is not orthogonal and the minimization mentioned above reduces to solving the following system of linear algebraic equations (SLAE)

$$\mathbf{V} = \mathbf{SB},$$

where $\mathbf{B}$ is a vector column of coefficients b_m, and the components of the vector $\mathbf{V}$ and the matrix $\mathbf{S}$ are equal respectively:

$$V_j = \int\limits_{\Phi} U(\varphi) G_j(\varphi)\, d\varphi, \qquad S_{jm} = \int\limits_{\Phi} G_j(\varphi) G_m(\varphi)\, d\varphi,$$

here

$$\int\limits_{\Phi} U(\varphi) G_j(\varphi)\, d\varphi = \sum_{m=1}^{M} b_m \int\limits_{\Phi} G_j(\varphi) G_m(\varphi)\, d\varphi, \quad j = 1, 2, \ldots, M. \tag{6}$$

The principal feature of SLAE (6) is their poor conditionality, which is a consequence of an attempt to solve an incorrect inverse problem. An increase in the stability of solutions can be achieved if the functions $G_m(\varphi)$ turns out to be orthogonal in the domain of Φ. In this case, in the matrix $\mathbf{S}$, only the elements on the main diagonal are different from zero and the coefficients b_m are easily found

$$\int\limits_{\Phi} U(\varphi) G_m(\varphi)\, d\varphi = b_m \sum_{j=1}^{M} G_j^2(\varphi)\, d\varphi, \quad m = 1, 2, \ldots, M.$$

Thus, the problem arises of choosing such an orthonormal in the domain of Φ systems of functions $\widetilde{g}_m(\varphi)$, images $\widetilde{G}_m(\varphi)$ of which are orthogonal in Φ.

4. SIMULTANEOUS ORTHOGONALIZATION OF THE SYSTEMS OF FUNCTIONS USED

The orthogonal functions $g_m(\varphi)$ and $G_m(\varphi)$ can be used as their own functions and IE (1). However, the numerical search for each of them boils down to solving unstable problems and, consequently, to the appearance of significant errors in solving the entire problem. Even in the

simplest case of searching for eigenfunctions, when the core of the IE is degenerate, i.e. DP of the $f(\varphi)$ measuring system is the DP of a one-dimensional antenna array (AA) [29]

$$f(\varphi) = \sum_{n=-K}^{n=K} j_n \exp(-ikdn \sin\varphi). \tag{7}$$

The SLAE obtained for searching for eigenfunctions turn out to be poorly conditioned. In (7) it is indicated: j_n is the magnitude of the current at the nth emitter, d is a distance between neighboring emitters, $2K+1$—the number of DP elements and the constant $k = 2\pi/\lambda$, where the wavelength $\lambda = 2\pi c/\omega$, c is the speed of light, ω is the frequency of radiation. It is significant that the conditionality numbers of the corresponding matrices increase exponentially with an increase in the number of eigenfunctions to be determined, i.e. with attempts to increase the effective angular resolution.

Note that the construction of an orthogonal system of functions $\widetilde{G}_m(\varphi)$ in the domain Φ can also be carried out on the basis of the Gram–Schmidt orthogonalization process. In this case, however, the resulting functions turn out to be images of functions that are not orthogonal in the domain of Φ. In this case, the source is also represented as a superposition of non-orthogonal functions, which significantly reduces the quality of the approximate solution.

The actual problem of simultaneous orthogonalization of systems of functions g_m and G_m is proposed to be solved on the basis of the following theorem, the proof of which is given in Appendix.

Theorem 1. *Let's define a system of N orthonormal functions $g_m(x)$ (hereafter $m = 1, 2, \ldots, N$) on the segment L_g and an arbitrary linear operator $\mathbf{A}$ generating a system of N functions $G = \mathbf{A}g$, on the segment L_G. Here G and g are N-dimensional vector columns with components G_m and g_m. Then there is a linear transformation, represented as a matrix $\mathbf{T}$, such that the systems of functions*

$$\widetilde{G}_m(\varphi) = \sum_{j=1}^{N} T_{jm} G_j(\varphi), \quad \widetilde{g}_m(\varphi) = \sum_{j=1}^{N} T_{mj} g_j(\varphi) \tag{8}$$

on the segments L_G and L_g, respectively, turn out to be orthogonal, while maintaining the condition $\widetilde{G} = \mathbf{A}\widetilde{g}$.

The results of the theorem allow us to simultaneously present the desired solution $I(\varphi)$ of the inverse problem under consideration and the signal under study $U(\varphi)$ in the form of decompositions over systems of orthogonal functions, which simplifies the analysis of the problem, increases the stability of numerical solutions and, ultimately, allows to increase the achieved degree of superresolution.

Using (A.1)–(A.5) (see Appendix), we obtain

$$\widetilde{G}_m(\varphi) = \int_{\Omega} f(\varphi - \phi)\widetilde{g}_m(\phi)\, d\phi, \qquad \widetilde{g}_m(\varphi) = \sum_{j=1}^{N} T_{mj} g_j(\varphi). \tag{9}$$

Further, expressing the received signal in the form of decomposition

$$U(\varphi) \cong \sum_{m=1}^{N} C_m \widetilde{G}_m(\varphi),$$

we find, due to the orthogonality of the functions, the coefficients C_m

$$C_m = \frac{1}{P_m} \int_{\Phi} U(\varphi)\widetilde{G}_m(\varphi)\, d\varphi, \quad \text{where} \quad P_m = \int_{\Phi} \widetilde{G}_m^2(\varphi)\, d\varphi. \tag{10}$$

Taking into account the entered designations, the received signal (1) can be represented as follows

$$U(\varphi) = \int\limits_{\Omega} f(\varphi - \phi) I(\phi)\, d\phi \cong \sum_{m=1}^{N} C_m \widetilde{G}_m(\varphi) = \int\limits_{\Omega} f(\varphi - \phi) \left(\sum_{m=1}^{N} C_m \widetilde{g}_m(\phi) \right) d\phi. \qquad (11)$$

Equating the integral expressions in (11), we obtain a solution to the inverse problem under consideration in the form of decompositions both according to the introduced system of functions (A.5) and according to the original system of N functions (3)

$$I(\varphi) \cong \sum_{m=1}^{N} C_m \widetilde{g}_m(\varphi), \qquad I(\varphi) = \sum_{j=1}^{N} b_j g_j(\varphi), \qquad b_j = \sum_{m=1}^{N} C_m T_{mj}. \qquad (12)$$

Next, the algorithm uses an iterative process of increasing N to increase the degree of superresolution achieved until stable solutions can be obtained.

Since the inverse problem is considered, the solution of which, after parameterization, is reduced to a SLAE solution, all the negative properties of inverse problems are preserved and transferred eventually to SLAE solutions. In the problems under consideration, the second and third signs of the correctness of the Hadamard problem are violated, namely: unambiguity of solutions and their stability. The matrices $\mathbf{S}$ in (6) turn out to be poorly conditioned. When trying to increase the resolution, the dimension of the $\mathbf{S}$ matrices increases, while the conditioning numbers increase exponentially and reach huge values: 10^{10}–10^{13}, so even insignificant rounding errors lead to inadequate solutions. The presence of noise and measurement errors further worsens the situation. The direct solution of SLAE by known numerical methods of linear algebra does not lead to a satisfactory result.

At the same time, the values of the conditioning numbers of matrices of type $\mathbf{T}$ from (8), (9) are many times—and the orders are less than those of matrices $\mathbf{S}$. This circumstance is an indicator of the higher stability of solutions obtained on the basis of Theorem 1, in comparison with the direct solution of SLAE (5), (6). Thus, the proposed approach to solving the problem (1) provides the opportunity to use a larger number of functions in the solution representation (12) compared to (3)–(6), which increases the angular resolution. In an alternative formulation, the developed approach makes it possible to achieve the same level of exceeding the Rayleigh criterion as other methods, but at a significantly higher level of noise and interference.

5. EXAMPLES OF PROBLEM SOLUTIONS

Initially, single-stage functions were selected to represent the solution in the domain $\Omega = [-\theta_0, \theta_0]$, where $2\theta_0 = \theta_{0.5}$, and the solution was searched based on the algebraic method briefly described above (3)–(5). Then the search for solutions was carried out on the basis of Theorem 1 and the relations (8)–(12), and the solutions obtained were compared.

Figure 1a of the five original functions $g_m(\varphi)$, $m = 1, \ldots, 5$, three are shown—$g_1(\varphi), g_2(\varphi)$ and $g_4(\varphi)$. Figure 1b shows for illustration the transformed modifications of the original functions $g_1(\varphi)$ and $g_4(\varphi)$, i.e. $\widetilde{g}_1(\varphi)$ and $\widetilde{g}_4(\varphi)$. Figure 2a shows the images of $G_m(\varphi)$ source functions $g_m(\varphi)$ at $m = 1, 3, 5$, and in Fig. 2b—images of $\widetilde{G}_m(\varphi)$ functions $\widetilde{g}_m(\varphi)$ in the domain Φ.

Two point targets with the same amplitude of the emitted signal were selected as classical objects for the study of resolution. The distance between the objects was consistently reduced until it was possible to obtain sufficiently stable solutions adequate to the original objects. When objects approach each other, false sources begin to appear in the solution. Their intensity increases dramatically with further convergence. Figure 3b shows the extreme case when they can still be neglected.

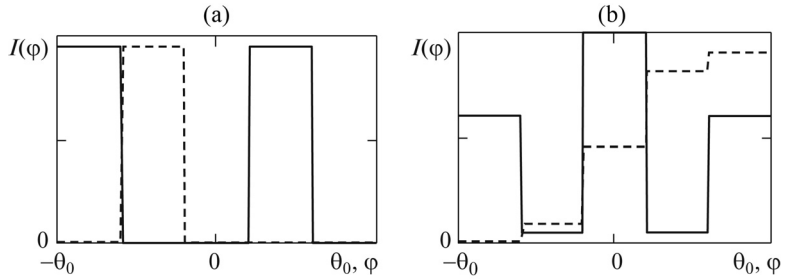

Fig. 1. Initial step functions (a), modified functions (b).

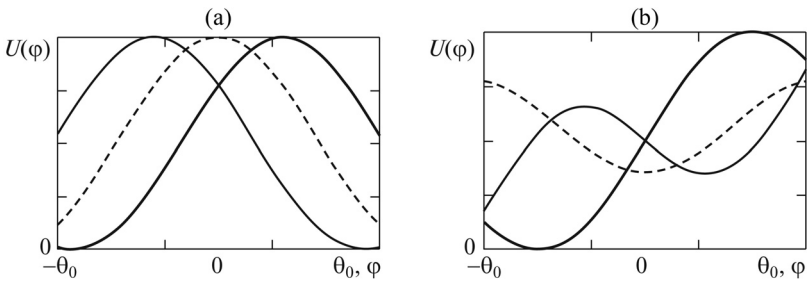

Fig. 2. Images of G_m original functions (a), images of $\widetilde{G}_m$ modified functions (b).

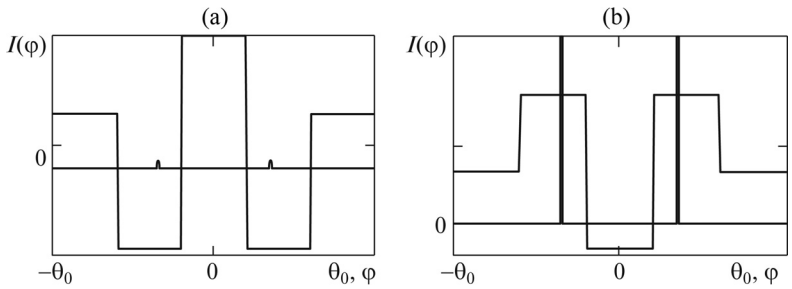

Fig. 3. Solution based on the original functions (a), solution based on modified functions (b).

Figures 3a and 3b present the solutions obtained in accordance with (3)–(6), i.e. without orthogonalization of functions and their images, as well as solutions after the procedure of simultaneous orthogonalization of $g_m(\varphi)$ and $G_m(\varphi)$. The angular position of point objects is shown as a bold vertical line, and the solution is shown as a polyline.

The results of numerical experiments have shown that by simultaneous orthogonalization it is possible to exceed the Rayleigh criterion four times (Fig. 3b). An attempt to obtain a stable solution to the same problem in accordance with (3)–(6) does not lead to a satisfactory result. The resulting inadequate solution, shown in Fig. 3a, is characterized by an oscillating character with a very large oscillation amplitude. Against the background of this solution, the true objects depicted on the same scale as in Fig. 3b are almost invisible. The type of solution is typical for cases when it is not possible to find an adequate solution. The conditioning numbers of the matrices used in solving and characterizing the stability of problems differ in the presented examples by two orders of magnitude.

It should be noted that when the number of M functions of the original system used in the solution representation (3) changes, the systems of functions $g_m(\varphi)$ and $G_m(\varphi)$ (9) themselves change. This feature has little effect on the running time of the program, since the basic calculations are performed using standard high-speed and well-developed algorithms.

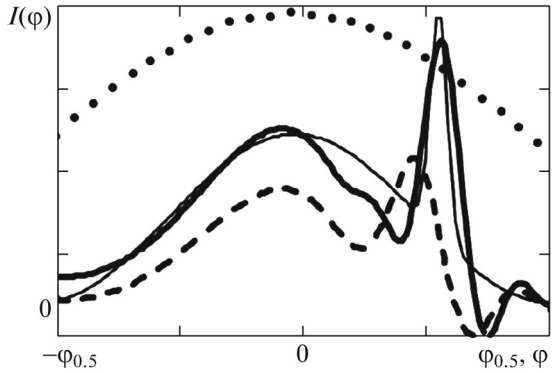

Fig. 4. A solution based on DOG wavelets.

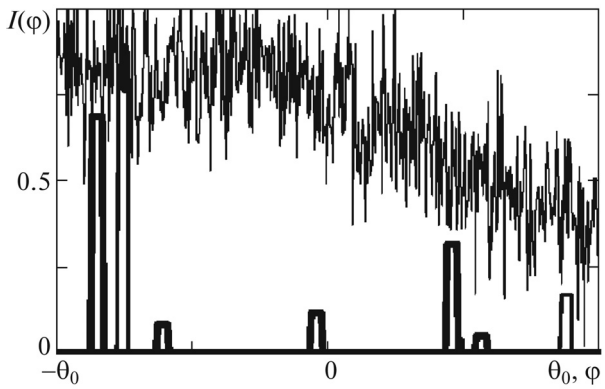

Fig. 5. A solution based on delta functions.

The choice of the initial system of functions $g_m(\varphi)$ is based on a priori information about the solution [16] and the shape of the signal received during scanning (1). Such information may include, in particular, the size and location of the signal source localization area, monotony, smoothness of the continuity area of the angular distribution of the amplitude of the emitted signal, the presence of areas with a discrete distribution, the dynamic range of intensity variation, restrictions on the gradient and other characteristics [11, 13, 16].

Figure 4 shows the solution of the inverse problem under consideration using this kind of a priori information. It was known that in the remote sensing problem, the reflecting surface is described by a smooth function with a smooth change in the amplitude of the reflected signal, with the possible presence of a small-sized area with high reflection. Based on this information, a system of functions based on DOG-wavelets was chosen to represent the solution.

Under direct observation without the proposed digital processing, the presented section has some averaged amplitude – the upper point curve. Signal processing by the algebraic method made it possible to identify the details of the amplitude distribution of $I(\varphi)$. In the form of a solid thin curve, Fig. 4 shows the true distribution of the reflected signal, the strokes represent the solution found by the algebraic method (3)–(6), the solid bold curve is the solution obtained using the considered double orthogonalization method.

Digital processing based on double orthogonalization has improved the quality of the solution, especially in the area of the area with a high gradient of the reflection coefficient.

Orthogonalization of function systems allows not only to increase the angular resolution, but, due to good stability, to obtain adequate solutions at high levels of random components.

Figure 5 shows the solution of the problem at a high noise level in the form of a bold polyline. The signal source consisted of two small-sized objects shown in the drawing with a thin polyline. The amplitudes of the signals reflected from the objects differed by five times. The objects were not resolved under direct observation. To illustrate, the figure shows the signal received during scanning in the Ω sector—the upper curve.

To represent solutions as a $g_m(\varphi)$ system, there was selected a system of delta functions located at the same distance from each other. In the process of finding a solution, these distances could be changed.

In the course of numerical experiments, the minimum value of the signal-to-noise ratio (SNR) was sought, at which it was still possible to obtain a satisfactory solution. The large difference in the amplitudes of the reflected signals significantly complicated the solution of the problem. False objects appeared, albeit with a small amplitude, the magnitude of which allowed them to be neglected when presenting the final solution. As a result, a completely satisfactory stable solution was obtained with a SNR equal to 1/3, or 10.5 dB. Many well-known methods, including [1–8], allow us to successfully solve such problems only with an SNR of at least 20 dB. Thus, the application of the method of simultaneous orthogonalization of systems of functions for solving inverse problems makes it possible to detail images of objects with an angular resolution exceeding the Rayleigh criterion at a significant level of random components of the signal. A further increase in the achieved degree of superresolution is possible with a decrease in the level of random components—noise in the studied signals.

6. IMPROVING THE SNR FOR UWB SYSTEMS

Currently existing UWB signal generation systems do not have sufficient energy to carry out measurements at significant distances [17–19]. In these conditions, an important task is to increase the range of systems by optimizing the digital processing of received UWB pulses. Optimization consists in the development of algorithms to increase the SNR in the received signals, which ultimately increases the range of the systems, and also improves the quality of images of objects with angular superresolution. Increasing the SNR increases the stability of solutions to the inverse problems discussed above, which are significantly more sensitive than direct ones to the presence and level of random components in the studied signals. Any linear algorithms for processing UWB signals that increase the SNR simultaneously provide an increase in the effective angular resolution.

Known methods of calculating characteristics and optimizing them are of little use for solving problems of optimizing the characteristics of UWB radars [20–28]. When emitting, receiving and reflecting ultra-wideband pulses from objects, it is necessary to take into account the dispersion dependences of the reflection characteristics of the studied objects, as well as antenna systems. As a result of the dispersion, the shape and spectrum of the received pulse differ significantly from the emitted one, which makes it almost impossible to use traditional methods of coherent signal processing.

Another feature of solving problems of analysis and optimization of UWB pulses is the difficulty of using well-developed spectral analysis methods in calculations, since for their successful application it is necessary to set the amplitude and phase spectra of pulses with high accuracy. The UWB signal, however, has an ultra-wide frequency band and, consequently, the spectral density of the pulse turns out to be small (often close to the magnitude of errors in calculations and measurements). In particular, when receiving a signal, its spectral density is often lower than the spectral density of noise. Under these conditions, the measurement accuracy of the amplitude-phase spectrum required for optimization cannot be achieved.

To overcome such difficulties, it is proposed to apply to calculations related to the description of the processes of radiation, reception, reflection and processing of UWB pulses a time domain

analysis method based on the representation of antenna systems, reception, generation systems, etc., as linear systems described by pulse characteristics.

The proposed unconventional approach turns out to be more convenient and accurate, since when using it, it is necessary to know not the spectrum, but only the time dependence of the generated signal $U(t)$, which can be determined experimentally with sufficiently high accuracy.

7. OPTIMIZATION OF THE IMPULSE RESPONSE OF THE RECEIVING SYSTEM

Let's set the task of searching for the impulse response $h_r(t)$ of the receiving system, which ensures the maximum possible power gain—q^2. The shape of the generated UWB pulse $U(t)$, the DP of the transmitting and receiving antenna systems at each of the frequencies used are considered to be set—$f_e(\varphi,\omega)$ and $f_p(\varphi,\omega)$, as well as the complex frequency response of the reflection of the object—$R(\omega)$. The specified variance dependencies allow using the Fourier transform F[..] determine the pulse characteristics of radiation, reception and reflection of the signal:

$$h_e(\varphi,t)=\mathbf{F}[f_e(\varphi,\omega)],\quad h_p(\varphi,t)=\mathbf{F}[f_p(\varphi,\omega)],\quad h_R(t)=\mathbf{F}[R(\omega)]. \tag{13}$$

In addition to the above characteristics, for modern systems based on antenna arrays (AA), it is necessary to additionally take into account the mutual influence of emitters on each other. Mutual influence is usually described using mutual complex resistances, i.e. the intrinsic resistance of the emitter changes by the amount of a certain introduced resistance. This resistance, called mutual resistance, depends on the distance between the emitters, measured by the ratio of the physical distance to the wavelength—the electrical distance. Without taking into account the mutual influence for narrow-band AA, the error in calculating their characteristics is 3–6% and it can often be neglected. When using UWB pulses for low-frequency components, the electrical distances between the emitters decrease several times and the resistance value increases noticeably. In order to avoid significant errors—up to 40–50%—mutual influence must be taken into account when constructing the pulse characteristics of UWB radars.

For two separate AA emitters numbered m and n located at a distance of $d_{m,n}$ from each other with co-directional DP, their mutual complex resistance

$$z(kd_{m,n})=r(kd_{m,n})+ix(kd_{m,n}),$$

expressed as [29]

$$r(kd_{m,n})=\frac{1}{B}\int_0^{\pi}\int_0^{2\pi}\phi_m(\varphi,\theta)\phi_n^*(\varphi,\theta)\cos\left(kd_{m,n}\sin\theta\right)\sin\theta\,d\varphi\,d\theta, \tag{14}$$

$$\begin{aligned}x(kd_{m,n})&=\frac{4}{kd_{m,n}}\int_0^{\pi}\phi_m(\theta)\phi_n^*(\theta)\,d\theta\\&-\int_0^{\pi}\int_0^{2\pi}\phi_m(\varphi,\theta)\phi_n^*(\varphi,\theta)\sin\left(kd_{m,n}\sin\theta|\sin\varphi|\right)\sin\theta\,d\varphi\,d\theta,\end{aligned} \tag{15}$$

where B is the normalizing factor, $\phi_m(\varphi,\theta)$—DP of a separate emitter.

Usually, the weakly directional DP of individual AA emitters are the same and often, especially for flat and linear AA, do not depend on the azimuth angle. Then they can be described with high accuracy in the form of functions $\phi(\varphi,\theta)=\cos^{\nu}\theta$ or a superposition of similar functions, where the parameter ν describes the directivity of the emitter. In this case, the integrals in (14), (15) are

taken explicitly [29], and the mutual effective resistance of two adjacent radiators (14) turns out to be equal

$$r(kd_{m,n}) = \Gamma(\nu + 3/2)\frac{J_{\nu+1/2}(kd_{m,n})}{(kd_{m,n}/2)^{\nu+1/2}}, \tag{16}$$

where $\Gamma(\nu)$ is a Gamma function, J_ν is a Bessel function of the order of ν. The mutual reactive part of the resistance, normalized to its own resistance, is reduced to the form

$$x(kd_{m,n}) = \frac{2\Gamma(\nu + 3/2)}{\sqrt{\pi}\Gamma(\nu + 1)kd_{m,n}} - \frac{\Gamma(\nu + 3/2)H_{\nu+1/2}(kd_{m,n})2^{\nu+1/2}}{(kd_{m,n})^{\nu+1/2}}, \tag{17}$$

where H_ν is a Struve function of the order ν [30].

For large AA, one can ignore the edge effects and assume that all emitters are in the same conditions. Then the resistances of all emitters turn out to be the same, and taking into account the mutual influence of the emitters leads to the need to use instead of $h_{e,p}(\varphi, t)$ from (13)

$$h_{e,p}(\varphi, t) = \mathbf{F}\left[\frac{f_{e,p}(\varphi, \omega)}{z(\varphi, \omega)}\right], \tag{18}$$

where $z(\varphi, \omega)$—the resistance of the emitter at the frequency ω, taking into account the influence of all other emitters of the AA.

Let's find the frequency dependence of the emitter resistance $z(\varphi, \omega)$. To this end, let's first consider the linear AA. For large AA with a number of $2N + 1$ emitters focused in the direction of φ to the AA axis (7), active resistance $r(\varphi, \omega)$ of each element represents the following amount, which can be extended indefinitely with almost no error

$$r(\varphi, \omega) = \sum_{n=-N}^{N} r(kdn)\cos\left(kdn\sin\varphi\right) \approx \sum_{n=-\infty}^{\infty} r(kdn)\cos\left(kdn\sin\varphi\right). \tag{19}$$

The sum of the series (19) can be represented as a closed expression. To do this, you first need to find the sum of the next row

$$W = \sum_{n=1}^{\infty} \frac{J_\nu(x)}{(nx/2)^\nu}\cos(nx\sin\varphi), \tag{20}$$

which is called the generalized Schlemilch series [30]. Note that the values of the sum (20) are given in the reference books only for a few special cases. In general, the sum of the series is found in [22]. It is shown that under the condition $kd < 2\pi/(1 + \sin\varphi)$, which is true for AA, the sum of the generalized Schlemilch series is equal to

$$W = -\frac{1}{2\Gamma(\nu + 1)} + \frac{\sqrt{\pi}}{\Gamma(\nu + 1/2)x}\cos^{2\nu-1}\varphi. \tag{21}$$

Finally,

$$r(\varphi, \omega) = \frac{2\sqrt{\pi}\Gamma(\nu + 3/2)}{\Gamma(\nu + 1)kd}\cos^{2\nu}\varphi. \tag{22}$$

The imaginary part of the resistance of each element of a large linear AA has a representation

$$X = \sum_{n=-\infty}^{\infty} x(kdn)\cos(kdn\sin\varphi) \cong \sum_{n=-N}^{N} x(kdn)\cos(kdn\sin\varphi) \tag{23}$$

Numerical estimates (23) for various ν and kd from (17) show that the value of X for large linear AA turns out to be close to zero. Thus, the resistance of each element in the composition of a large linear AA $z(kd)$ with good accuracy takes the value (22), which allows us to find the impulse response (18).

The resistance of the radiator in a large flat AA is obtained twice using the sum (22)

$$r(\varphi,\omega)=\frac{4\pi(\nu+1/2)}{(kd)^2}\cos^{2\nu-1}\varphi. \tag{24}$$

Now, using the found resistance values, we find the pulse characteristics of the radiation and AA reception in the form (18).

Typically, the SNR for pulse signals is defined as the ratio of the square of the maximum value of the useful signal to the RMS value of the noise $\overline{U_n^2}$

$$q^2=\frac{U_M^2}{\overline{U_n^2}}. \tag{25}$$

Then for narrowband signals, when the frequency band is much less than the fundamental frequency $\Delta\omega\ll\omega_0$, for the viewing angle $\varphi=0$ we get

$$q^2=\frac{f^4(0,\omega_0)|R(\omega_0)|^2}{N_0(\omega_0)}, \tag{26}$$

where N_0 is the spectral density of noise at the frequency ω_0. For UWB signals, considering noise to be a stationary random process, (25) takes the form:

$$q^2=\frac{\left(\int_{-\infty}^{\infty}h_r(t)U_r(t_0-t)\,dt\right)^2}{\int_{-\infty}^{\infty}\int_{-\infty}^{\infty}h_r(t)h_r(T)K(t-T)\,dt\,dT}, \tag{27}$$

where $U_r(t)$ is the received signal, t_0 is the time when the useful signal reaches the maximum value of U_M, $K(t)$ is the autocorrelation function of noise at the receiver input. Often in practically significant problems, when noise can be described as white, the $K(t)$ function is a delta function. Then, solving the variational problem of finding $h_r(t)$ from (27), which provides the maximum possible value of q^2 up to a constant, we obtain

$$h_r(t)=U_0(t_0-t),\qquad U_r(t)=h_e(0)\star h_R(t)\star h_e(0)\star U_g(t), \tag{28}$$

where $U_g(t)$ is the generated signal, and the symbol $\star$ denotes the convolution of functions. Note that the first two convolutions are formed by the given functions and can be replaced by a single dependency

$$H_r(t)=h_e(0)\star h_R(t)\star h_e(0),\qquad U_r(t)=H_r(t)\star U_g(t), \tag{29}$$

which determines $h_r(t)$ from (28), which can be called the impulse response of the optimal filter (OF).

Most often, in communication, radar, and remote sensing tasks, noise is considered white. However, in an ultra-wide frequency band, the spectral noise density may differ markedly from the constant, and then its shape must be taken into account when synthesizing OF. In this case, instead of (29) from (27) up to a constant, it follows

$$U_r(t_0-t)=\int\limits_{-\infty}^{\infty}h_r(\tau)K(t-\tau)\,d\tau \tag{30}$$

and now, to determine $h_r(t)$ OF, it is necessary to numerically solve the resulting integral equation (30).

8. RESULTS OF NUMERICAL EXPERIMENTS

The problem of optimal reception of UWB pulses when reflected from an object with a smooth increase in the value of the modulus of the reflection coefficient from the frequency $R(\omega)$ was considered and a fast-variable phase characteristic. As the spectral noise density $N_0(\omega)$ the distribution of atmospheric noise in the wavelength range of 1 m–3 cm was chosen. The DP of the antenna system at each of the frequencies used corresponded to the DP of the antenna array with a beam width of $2\theta_0 = 3^\circ$ at the average frequency of the range used.

The results of solving the problem are shown in Fig. 6. Shows: the initial UWB pulse is a dashed curve; the received UWB pulse without using OF is a thin solid curve; the received UWB pulse after optimal processing in the receiver (28), (29) is a bold curve. Noticeable changes occur in the received signal due to dispersion: —the pulse duration increases significantly; —the maximum modulo values of the reflected signal, pronounced in the initial pulse, disappear; —the shape of the received pulse, and therefore the shape of its spectrum, become little similar to the generated signal.

The use of an optimal receiver for UWB signals turns out to be highly effective, since it is used in an ultra-wide frequency band. In the given example of optimization of reception from the direction $\varphi = 0$, the SNR increased by more than 150 times, which corresponds to an increase in the range of the system by 3.7 times.

When receiving a signal from a direction other than $\varphi = 0$, the filter characteristic $h_r(t)$ in accordance with (28)–(30) is no longer optimal and increases the peak value of the signal to a lesser extent than from the direction $\varphi = 0$. In the given example, the optimization gain for $\varphi = 0$ decreased by 5 times at the boundary of the transmitting beam $\varphi = \theta_0$. The revealed pattern with optimal filtering of UWB pulses shows that the effective width of the receiving DP for the signal in question becomes significantly less than θ_0. This effect can be used to improve the accuracy and angular resolution of UWB systems when searching and tracking objects with known reflection characteristics.

In practice, it is difficult to expect that the complex reflection coefficient of the object under study, especially its phase characteristic, is precisely known. However, as numerical experiments have shown, taking into account even partial information about the reflective properties of an object can significantly increase the SNR—up to 0.2–0.5 from the value of the optimal q^2. In the example given, the phase characteristic of the reflection was given as a very approximate estimate. Nevertheless, it was possible to significantly increase the SNR by about 50 times.

The obtained theoretical results and the results of numerical experiments on a mathematical model show that optimizing the reception of UWB pulses makes it possible to increase the probability of correct detection and identification of the objects under study.

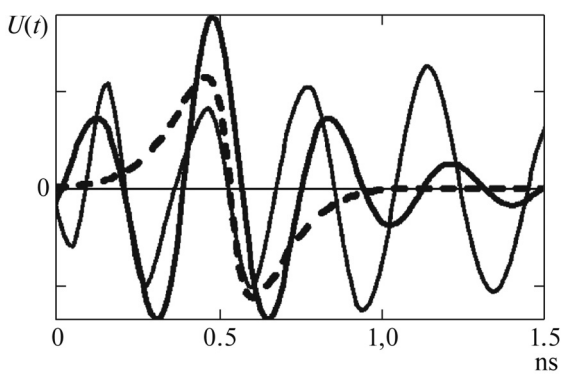

Fig. 6. The shapes of the generated and received UWB pulses.

9. CONCLUSION

1. The proposed methods of processing received signals based on the simultaneous orthogonalization of two interconnected systems of functions make it possible to increase the stability of the inverse problems being solved and restore the image of signal sources with an angular resolution several times higher than the Rayleigh criterion.

2. Algorithms based on algebraic methods make it possible to obtain satisfactory solutions with a signal-to-noise ratio of 15–20 dB, and sometimes at 11–12 dB, i.e. with significantly higher values of random components than the well-known methods described in domestic and foreign literature.

3. A priori information about signal sources allows for a targeted selection of systems of functions to represent solutions and, thereby, increase the adequacy and stability of the solutions obtained.

4. The relative simplicity of object image recovery algorithms makes it possible to use them in real time.

5. The variational problem of optimizing the pulse characteristics of the receiver of probing UWB pulses has been solved. The efficiency of using the proposed algorithms for processing UWB signals is shown, which allows 2–4 times to increase the range of UWB systems and improve the quality of radio images.

6. It is shown that optimizing the shape of the received UWB pulses allows for known object types to simultaneously increase the range of the systems, improve their angular characteristics and detection and identification characteristics.

FUNDING

The work was partially supported by the Russian Scientific Foundation, project no. 23-29-00448.

APPENDIX

Proof of Theorem 1. The system of functions $G_m(x)$ is generally non-orthogonal to L_G. Let's make a Gram matrix based on it, i.e. a matrix $\mathbf{P}$ of scalar products with elements P_{mn}:

$$P_{mn} = (G_m, G_n) = \int\limits_{\Phi} G_m(\phi) G_n(\phi)\, d\phi. \tag{A.1}$$

Since the matrix $\mathbf{P}$ is symmetric and positively defined, there is a transformation $\mathbf{T}$ that leads it to a diagonal form

$$\widetilde{\mathbf{P}} = \mathbf{T}^{\star}\mathbf{P}\mathbf{T}. \tag{A.2}$$

Using the found matrix $\mathbf{T}$, we introduce a new system of functions $\widetilde{G}_m(x)$ in the form (9). The resulting system turns out to be orthogonal on the segment L_G, which is easily verified by directly calculating scalar products:

$$(\widetilde{G}_m, \widetilde{G}_n) = \sum_{j,i=1}^{N} T_{jm} T_{in} \int\limits_{\Phi} G_j(\phi) G_i(\phi)\, d\phi = \sum_{j,i=1}^{N} T_{jm} T_{in} P_{ji} = \widetilde{P}_{mn},$$

where $\widetilde{P}_{mn}$ are the elements of the diagonal matrix (A.2).

Now let's find the system of functions $\widetilde{g}_m(x)$, which generates the resulting orthogonal in the domain L_G the system $\widetilde{G}_m(x)$, i.e.

$$\widetilde{G}_m = \mathbf{A}\widetilde{g}_m. \tag{A.3}$$

The required representation (9) follows

$$\widetilde{G}_m = \sum_{j=1}^{N} T_{mj} \mathbf{A} g_j = \mathbf{A} \left(\sum_{j=1}^{N} T_{mj} g_j \right). \tag{A.4}$$

Comparing (A.3) and (A.4), we obtain

$$\widetilde{g}_m(x) = \sum_{j=1}^{N} T_{mj} g_j(x). \tag{A.5}$$

The found system (A.5) turns out to be orthogonal on the segment L_g. Indeed, due to the orthogonality of the functions $g_m(x)$ and the orthogonality of the eigenvectors of the matrix $\mathbf{P}$ forming the matrix $\mathbf{T}$, we have

$$(\widetilde{g}_m(x), \widetilde{g}_n(x)) = \sum_{j=1}^{N} T_{mj} T_{nj} (g_j, g_i) = \left\{ \begin{array}{ll} 0, & m \neq n \\ \lambda_m, & m = n \end{array} \right. , \quad \lambda_m = \sum_{j=1}^{N} T_{mj}^2.$$

Note that the found system of orthogonal functions $\widetilde{g}_m(x)$ is determined by the same linear transformation $\mathbf{T}$ as the system of functions $\widetilde{G}_m(x)$.

As a result, based on a given system of N orthogonal functions $g_m(x)$ on the segment L_g, a new orthogonal system of functions on the same segment is constructed, generating an orthogonal system of functions $\widetilde{g}_m(x)$ in the domain L_g. The theorem is proved

REFERENCES

1. Odendaal, W., Barnard, E., and Pistorius, C.W.I., Two Dimensional Superresolution Radar Imaging Using the MUSIC Algorithm, *IEEE Trans.*, 1994, vol. AP-42, no. 10, pp. 1386–1391. https://doi.org/10.1109/8.320744
2. Waweru, N.P., Konditi, D.B.O., and Langat, P.K., Performance Analysis of MUSIC Root-MUSIC and ESPRIT DOA Estimation Algorithm, *Int. J. Electrical Computer Energetic Electronic and Communication Engineering*, 2014, vol. 08, no. 01, pp. 209–216.
3. Yuebo Zha, Yulin Huang, and Jianyu Yang, An Iterative Shrinkage Deconvolution for Angular Super-Resolution Imaging in Forward-Looking Scanning Radar, *Progress In Electromagnetics Research B*, 2016, vol. 65, pp. 35–48. https://doi.org/10.2528/PIERB15100501
4. Almeida, M.S. and Figueiredo, M.A., Deconvolving images with unknown boundaries using the alternating direction method of multipliers, *IEEE Trans. Image Process.*, 2013, vol. 22, no. 8, pp. 3074–3086.
5. Dudik, M., Phillips, S.J., and Schapire, R.E., Maximum entropy density estimation with generalized regularization and an application to species distribution modeling, *J. Machine Learning Research*, 2007, vol. 8, pp. 1217–1260.
6. Stoica, P. and Sharman, K.C., Maximum likelihood methods for direction-of-arrival estimation, *IEEE Trans. on Acoustics, Speech and Signal Processing*, 1990, no. 38(7), pp. 1132–1143.
7. Geiss, A. and Hardin, J.C., Radar super resolution using a deep convolutional neural network, *Journal of Atmospheric and Oceanic Technology*, 2020, vol. 37, no. 12, pp. 2197–2207.
8. Ramani, S., Liu, Z., Rosen, J., Nielsen, J., and Fessler, J.A., Regularization parameter for nonlinear iterative image restoration and MRI selection reconstruction using GCV and SURE- based methods, *IEEE Trans. on Image Processing*, 2012, vol. 21, no. 8, pp. 3659–3672.
9. Morse, P. and Feshbach, H., *Methods of Theoretical Physics*, New York: McGraw-Hill Book Company, Inc., 1953.
10. Lagovsky, B.A. and Rubinovich, E.Y., Algebraic methods for achieving super-resolution by digital antenna arrays, *Mathematics*, 2023, vol. 11, no. 4, pp. 1–9. https://doi.org/10.3390/ math11041056
11. Lagovsky, B.A., Samokhin, A.B., and Shestopalov, Y.V., Angular Superresolution Based on A Priori Information, *Radio Science*, 2021, vol. 56, no. 1, pp. 1–11. https://doi.org/10.1029/2020RS007100

12. Lagovsky, B.A., Angular superresolution in two-dimensional radar problems, *Radio Engineering and Electronics*, 2021, vol. 66, no. 9, pp. 853–858. https://doi.org/10.31857/S0033849421090102

13. Lagovsky, B.A. and Rubinovich, E.Y., Algorithms for digital processing of measurement data providing angular superresolution, *Mechatronics, automation, control*, 2021,vol. 22, no. 7, pp. 349–356. https://doi.org/10.17587/mau.22.349-356

14. Kalinin, V.I., Chapursky, V.V., and Cherepenin, V.A., Superresolution in radar and radiohologography systems based on MIMO antenna arrays with signal recirculation, *Radio engineering and electronics*, 2021, vol. 66, no. 6, pp. 614–624. https://doi.org/10.31857/s0033849421060139

15. Shchukin, A.A. and Pavlov, A.E., Parameterization of user functions in digital signal processing to obtain angular superresolution, *Russian Technological Journal*, 2022, no. 10(4), pp. 38–43. https://doi.org/10.32362/2500-316X-2022-10-4-38-43

16. Lagovsky, B.A. and Samokhin, A.B., Superresolution in signal processing using a priori information, *IEEE Conf. Publications International Conference Electromagnetics in Advanced Applications (ICEAA)*, Italy, 2017, pp. 779–783. https://doi.org/10.1109/ICEAA.2017. 8065365.

17. Dong, J., Li, Y., Guo, Q., and Liang, X., Through-wall moving target tracking algorithm in multipath using UWB radar, *IEEE Geosci. Remote Sens. Lett.*, 2021, pp. 1–5. https://doi.org/10.1109/lgrs.2021.3050501

18. Khan, H.A., Edwards, D.J., and Malik, W.Q., Ultra wideband MIMO radar, *Proc. IEEE Intl. Radar Conf. Arlington*, VA, USA, 9 May 2005.

19. Zhou Yuan, Law Choi Look, and Xia Jingjing, Ultra low-power UWB-RFID system for precise location-aware applications, *2012 IEEE Wireless Communications and Networking Conference. Workshops (WCNCW)*, 2012, pp. 154–158.

20. Taylor, J.D., *Ultra-wideband Radar Technology*, CRC Press Boca Raton, London, New Work, Washington. 2000.

21. Holami, G., Mehrpourbernety, H., and Zakeri, B., UWB Phased Array Antennas for High Resolution Radars, *Proc. of the 2013 International Symp. on Electromagnetic Theory*, 2013, pp. 532–535.

22. Lagovsky, B.A., Samokhin, A.B., and Shestopalov, Y.V., Pulse Characteristics of Antenna Array Radiating UWB Signals, *Proceedings of the 10th European Conference on Antennas and Propagation (EuCAP 2016)*, Davos, Switzerland, 2016, pp. 2479–2482. https://doi.org/10.1109/ EuCAP.2016.7481624

23. Lagovsky, B.A., Samokhin, A.B., and Shestopalov, Y.V., Increasing accuracy of angular measurements using UWB signals. 2017 11th European Conference on Antennas and Propagation (EUCAP), *IEEE Conf. Publications. Paris*, 2017, pp. 1083–1086. https://doi.org/10.23919/ EuCAP.2017.7928204

24. Anis, R. and Tielert, M., Design of UWB pulse radio transceiver using statistical correlation technique in frequency domain, *Advances in Radio Science*, 2007, vol. 5, pp. 297–304. https://doi.org/10.5194/ars-5-297-2007

25. Niemela, V., Haapola, J., Hamalainen, M., and Iinatti, J., An ultra wideband survey: Global regulations and impulse radio research based on standards, *IEEE Communications Surveys and Tutorials*, 2016, vol. 19, no. 2, pp. 874–890. https://doi.org/10.1109/COMST.2016.2634593

26. Barrett, T., History of UWB Radar and Communications: Pioneers and Innovators, *Progress in Electromagnetics Symposium (PIERS) 2000. Microwave Journ*, January 2001.

27. Dmitriev, A.S., Efremova, E.V., and Kuzmin, L.V., Generation of a sequence of chaotic pulses under the influence of a periodic signal on a dynamic system, *Letters to the Journal of Theoretical Physics*, 2005, vol. 31, no. 22, p. 29. https://doi.org/10.1134/ S1064226906050093

28. Yang, D., Zhu, Z., and Liang, B., Vital sign signal extraction method based on permutation entropy and EEMD algorithm for ultra-wideband radar, *IEEE Access*, 2019, vol. 7. https://doi.org/10.1109/ACCESS.2019.2958600.

29. Vendik, O.G., *Antenny s nemekhanicheskimi dvizheniyami lucha* (Antennas with non-mechanical beam motion), Moskow: Sov. Radio, 1965.

30. Watson, G.N., *Theory of Bessel functions*, trans. from the 2nd English edition, Moscow: IL, 1947.

This paper was recommended for publication by A.A. Bobtsov, a member of the Editorial Board